High Speed Spherical Roller Bearing Analysis and Comparison with Experimental Performance*

Robert J. Kleckner† and George Dyba†

The general class of load support systems consists of mechanical assemblies which transfer force and moment vectors. The transfer is constrained to maintain component displacements within prescribed, and frequently severe, limits.

Rolling-element bearings are a subset of this general load support system class, characterized by high load carrying capacity, low power loss, stability during load fluctuations and rotation reversal, and tolerance of start-stop operation. Various rolling-element-bearing configurations are contained within this subset to service specific application requirements. The ball bearing, for example, supports combined direction loading and tolerates some misalinement. They do so at a penalty because elements with "line" in comparison with "point" contact conjunctions offer superior capacity for a given design volume (fig. 1). However, bearings having tapered and cylindrical roller geometries with "line" contact are less tolerant of misalinement.

The relative displacement of components is an inescapable physical reality when mechanical assemblies transfer force. Typically, structural elements distort within the generally asymmetric assembly, causing a misalinement of bearing raceways. This departure from the idealized "rigid" assembly can be compensated for but not eliminated by manufacture, assembly, and operation. In the presence of such deflections, and resulting misalinement, line-contact geometries can be optimized only for a specific single-load condition (ref. 1). Severe penalties, including loss of bearing life and operating performance, result for off-optimum load support.

The self-alining spherical roller bearing (fig. 2) answers some shortcomings of the configurations noted above. The geometry is unique. At low loads, the load vector is transferred by point contacts. At higher loads, modified line contacts perform this function. The bearing also supports combined radial and axial loading. This versatility has led to successful implementation in the large load support systems required by the steel, paper, and marine industries. Successful application has also been achieved in high-reliability mechanical assemblies, such as airborne planetary gear reduction sets.

The rolling-element bearing subset of the load support system class, in today's technology, is being required to operate at ever increasing DN values. Ball and cylindrical bearings, for example, have seen numerous applications at the 3.0 MDN[1] level. Tapered bearings are being asked to follow in this regime. These new demands result from the requirements posed by advanced hardware missions and the increased emphasis on extracting maximum energy from a given process cycle. Basic thermodynamics, particularly in mobile powerplant design, dictates higher temperatures, stresses, and speeds. Simultaneously, the assembly is required to occupy a smaller volume and weigh less. The combination of these parameters defines a lighter assembly, under increased stress, in a high-temperature environment. The bearings which reside in assemblies of decreased structural rigidity, must sustain high combined loads under conditions of misalinement and, furthermore, do so at higher speeds.

The conventional spherical rolling-element bearing design meets all but one of the challenges posed by these emerging requirements. Operating speed has been restricted to maximum DN values of about 0.4 MDN. Efforts are now under way to reach higher speeds. Particular emphasis is placed on reaching a 1.0 MDN value.

*This work done under NASA contract NAS3-20824.

†SKF Industries, Inc.

[1]The term MDN refers to million DN, where DN is the bearing bore in mm times the speed in rpm. For the 40-mm-bore bearing test case, 0.8 MDN is approximately 4 times the catalog maximum speed limit.

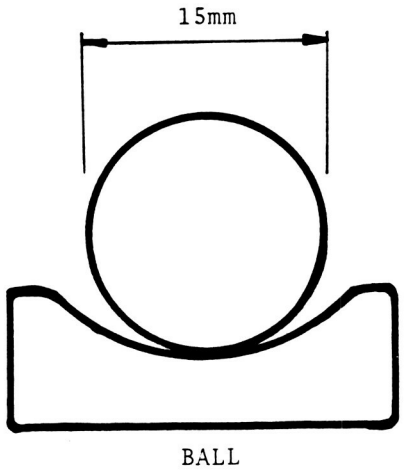

BALL

POINT CONTACT CAPACITY
= 22,240 N (5000 lbs)

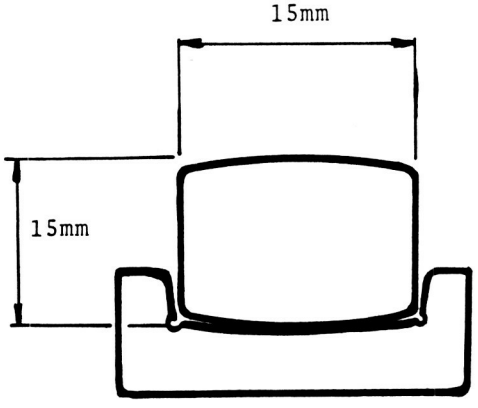

SPHERICAL

MODIFIED LINE CONTACT CAPACITY
= 36,200 N (8,140 lbs)

Figure 1. - Example of capacities of line and point contacts.

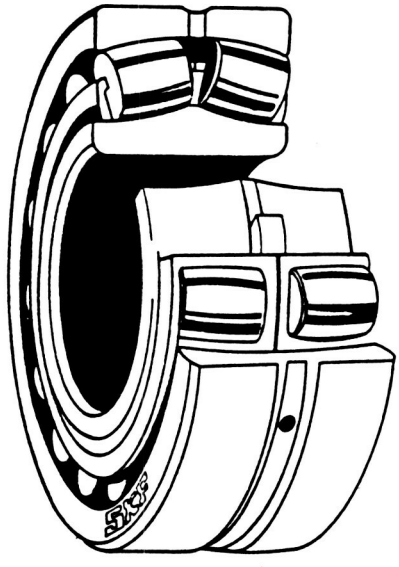

Figure 2. - Typical spherical rolling-element bearing geometry.

The need to extend the operating DN regime for spherical roller bearings requires a realistic assessment of current methods for their design. Examination reveals that the contemporary design relies on "rules," hand calculations, and some modest computerized simulations. The presence of mandated safety factors in these rules for successful application reveals the measure of design performance buffers. At the same time, it reveals an opportunity for increasing performance and thus DN values to satisfy emerging load support needs.

Practical use of design reserves requires a more detailed understanding of and the ability to predict bearing performance within a load support system. The complexity of the interactions between the bearing and its environment requires an analytic/design tool to describe the thermomechanical dialogue present (ref. 2). Such a simulation tool can be created using high-speed digital computers.

Several investigators have addressed the analysis of spherical roller bearings, setting the stage for the required computerized simulation. Recently, Kellstrom (ref. 3) explored the fundamental mechanics that control symmetric roller behavior. He specifically addressed roller "self-guidance" and explored the optimization of their skewing angles to minimize heat generation. Wieland and Poesl (ref. 4) have presented an interpretation of the empirical state of the art in spherical roller bearing design and application. Harris and Broschard (ref. 5) as well as Liu and Chiu (ref. 6) have examined these bearings in planetary-gear applications in earlier investigations. Palmgren (ref. 7) and Harris (ref. 8) touch on computational procedures. Manufacturers' catalog data and popularized applications articles further serve to highlight the need for a thorough analytic examination of the coupled phenomena which occur during spherical roller bearing operation.

This paper describes the capabilities of a spherical roller bearing analysis/design tool, Spherbean (spherical bearing analysis). Capabilities of the analysis are demonstrated then verified by comparison with experimental data. A practical design problem is presented where the computer program is used to improve a particular bearing's performance (refs. 9 to 11).

Program Description

Spherbean (refs. 9 to 11) has been created to simulate the performance of double-row spherical roller bearings under a variety of operating conditions (fig. 3). Emphasis has been placed on detailing the effects of roller skew, roller-end-to-flange contact, and change in clearance as a function of speed, interference fit, and temperature.

The complete range of EHD contact considerations has been treated in the computation of raceway and flange contact detail. A flexible outer-ring analysis is among the several options made available to address special applications (fig. 3). For simulation of planet bearing performance, where the bearing's outer ring is integral with the planet gear (fig. 4), the carrier speed is considered in the computation of bearing kinematics. The user can choose the capabilities to be activated in a given simulation, or let the program default to a "standard" configuration. Spherbean also checks user-supplied data for magnitude and consistency. A failed check results in a diagnostic abort message.

Program capabilities also include both time transient and steady-state temperature mapping of a spherical bearing system. This option permits exploration of the bearing's temperature as a function of speed. When coupled with the option to compute the bearing's operating clearance, thermally induced bearing seizure can be examined. Activating the time transient thermal analysis allows the user to follow the system temperature rise and bracket the time-to-failure after loss of lubricant, for example.

Demonstration of Capabilities

The program's thermal option is illustrated in the following steady-state analysis of a 40-mm-bore bearing to 20 000 rpm. Program results are then compared with instrumented test results.

USER MUST PROVIDE

LOAD VECTOR FX, FY, FZ

OPERATING SPEED

GEOMETRY { ROLLER, RACEWAYS, FLANGE, CAGE }

USER OPTIONALLY PROVIDES

INTERFERENCE FIT DATA

PLANET GEAR BEARING DATA

SYSTEM DESCRIPTION FOR TEMPERATURE CALCULATIONS

SPLIT CAGE DATA

LUBRICANT PROPERTIES

MATERIAL PROPERTIES

Figure 3. - User supplied data requirements.

Test Rig and Subsystems

The experimental data used for comparison were generated on the spherical bearing test rig[2] (fig. 5). The rig has the capability to load the specimen both axially and radially at inner ring speeds to 20 000 rpm. Instrumentation is provided to measure the bearing oil-in and oil-out temperatures, inner- and outer-ring temperatures, inner-ring and cage speeds, operating torque, oil flow rates, and the operating parameters of secondary equipment.

Lubrication is provided to the test bearing at 93° C by way of a circumferential groove in the outer ring where it enters the bearing cavity through three radial holes. The lubricant used in all tests was a type II ester, conforming to the MIL-L-23699 specification.

The test rig consists of a hollow rectangular housing, which accommodates a solid shaft, support bearings, and lubrication rings, which direct recirculating oil into one side of each support bearing at three equally spaced locations.

The shaft extends from both ends of the housing through labyrinth seals. The test bearing is mounted on one end of the shaft extension. The other end is attached to a flexible quill. The quill is attached to either a jack shaft (for low-speed operation) or a gear box (for high-speed operation). The jack shaft or gear box is driven through a belt and pully arrangement by a variable-speed motor.

The test bearing inner ring is mounted to the shaft with an interference fit and clamped between a shoulder and an end cap. The shaft section located under the test bearing is hollow to accommodate the circuitry for the resistance temperature detectors (RTD's) mounted in slots machined into the shaft surface.

The outer ring of the test bearing is mounted in a housing which doubles as the inner ring of a radial hydrostatic bearing. The outer ring of the radial hydrostatic bearing contains the oil supply holes, restrictors, and bearing pads. The hydrostatic bearing outer ring is attached to a hydraulic ram that applies the radial load through the center of the test bearing.

The test bearing is enclosed on the inboard side by a faceplate mounted to the housing, which forms a labyrinth seal around the shaft. The outboard enclosure is formed by a spherical segment

[2]Details of the test facility were documented by Rosenlieb (ref. 12).

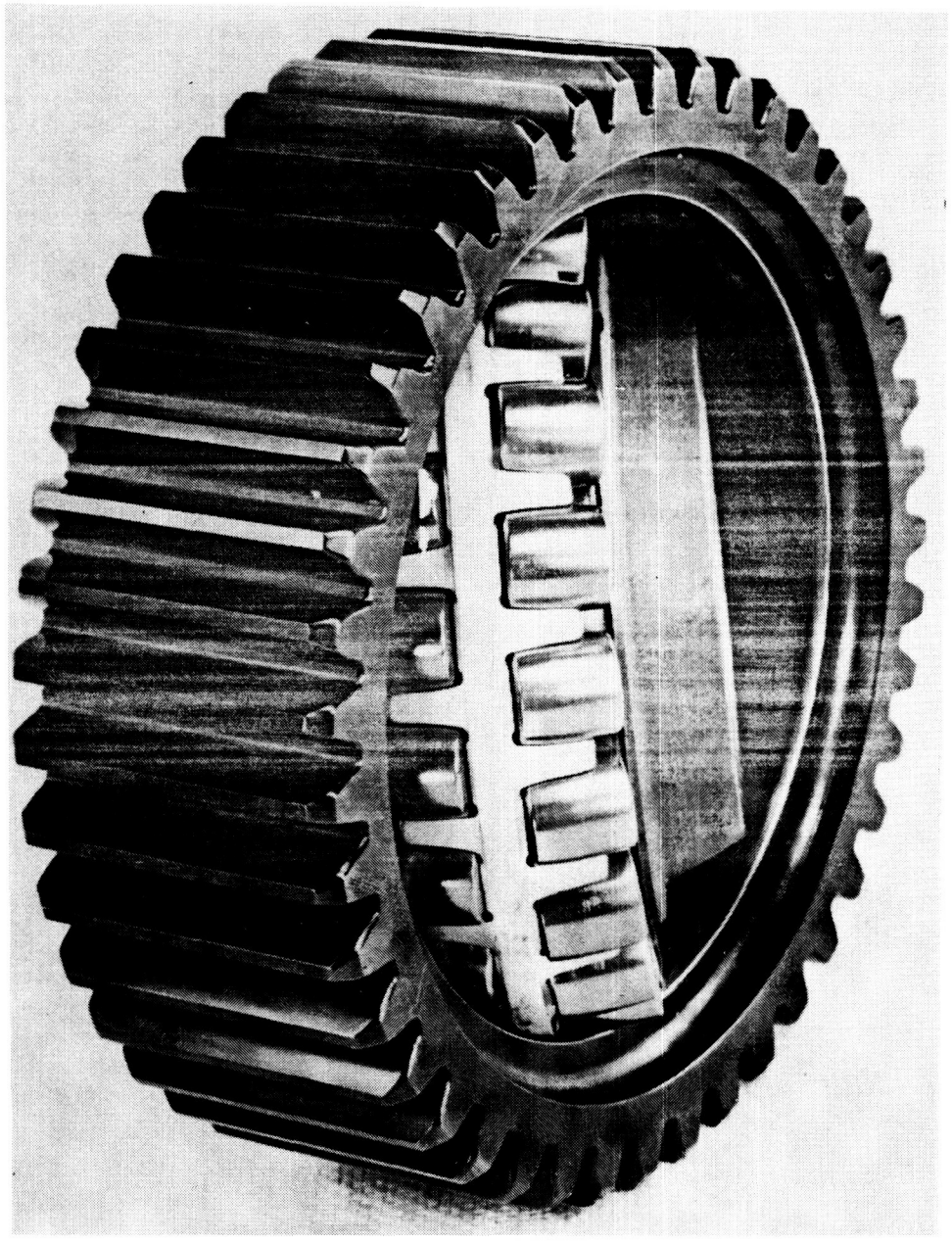

Figure 4. - Spherical roller planet bearing.

which doubles as the face plate of an axial hydrostatic bearing. The axial hydrostatic block, containing the oil supply holes, restrictors, and pads, has a matching contour. Axial load is applied to the bearing by a hydraulic ram located on an angle bracket bolted to the rig's foundation.

Test Rig System Model

Test rig geometry and material properties were used to reduce the configuration to an equivalent, cross-coupled, lumped-mass nodal network containing 50 temperature nodes. Of these, the temperatures of 44 nodes are determined by Spherbean, and the remaining six are specified as system boundary conditions.

Figures 6 and 7 show the extent of the test rig that was thermally simulated. The model is bounded on the left (nodes 1, 21, and 47 in fig. 6) by the axial hydrostatic bearing and ambient air.

The actual test rig continues past this point in the form of (thermally) minor support hardware for the thrust bearing and a rotary transformer drive quill. Approximately 50 percent of the quill was modeled, since its diameter (7 mm) is small in comparison with the test bearing bore (40 mm), and, therefore, contributes very little to the overall heat balance within the rig.

The thermal model is bounded on the right side by a support cylindrical roller bearing. The support bearing model was included to increase the accuracy of the predicted test bearing inner-ring temperatures, since the test bearing thermally communicates with the support bearing by transferring heat through the drive shaft.

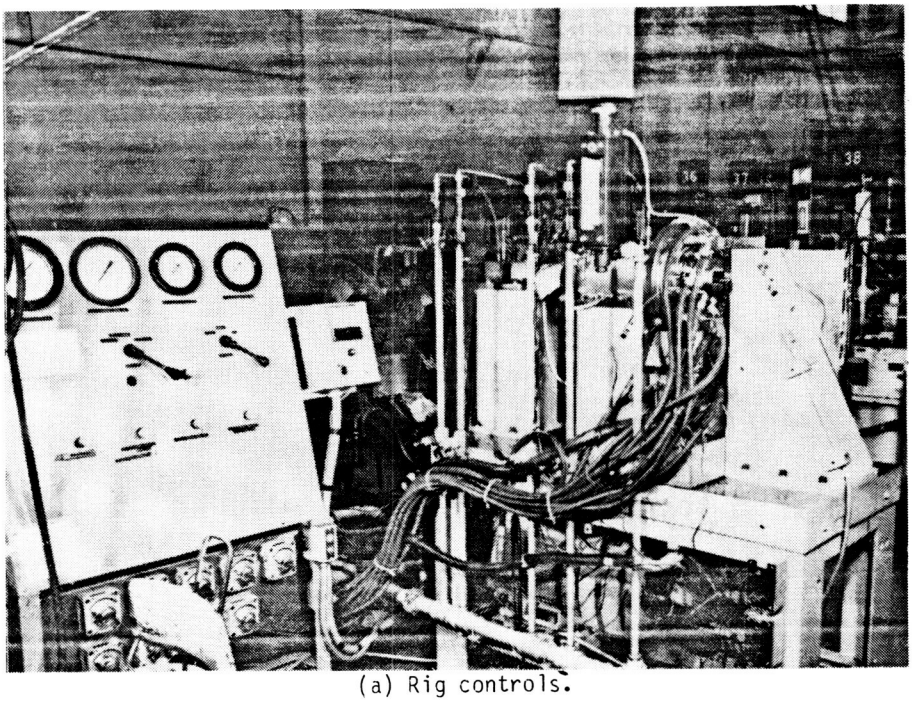

(a) Rig controls.

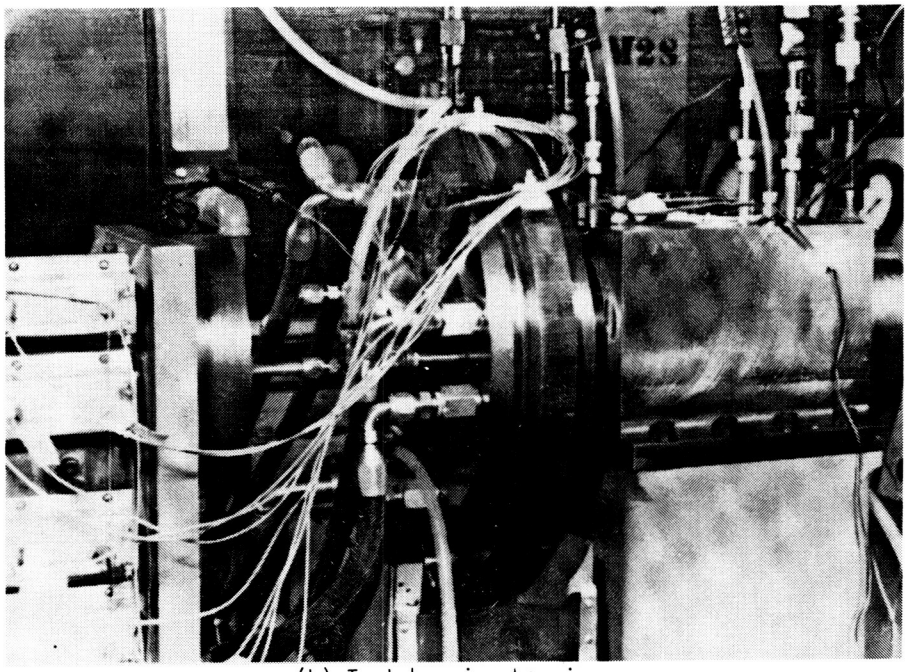

(b) Test bearing housing.

Figure 5. - High-speed test rig.

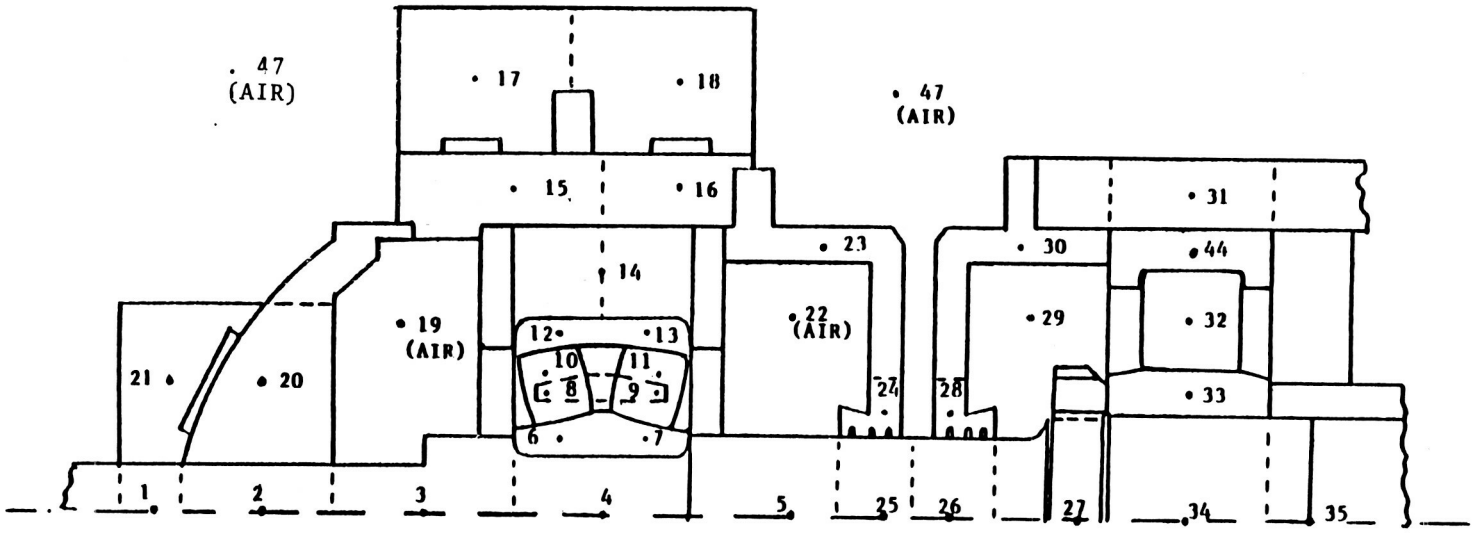

Figure 6. - System model; metal and air nodes.

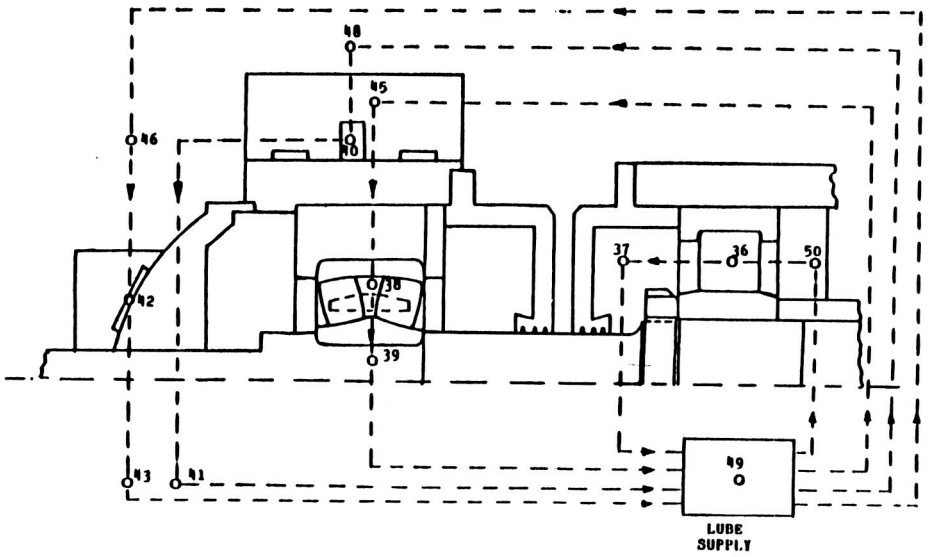

Figure 7. - System model; lubricant system nodes

Three sources of heat generation, other than the test bearing, were considered. These are two labyrinth seals, located at nodes 24 and 28, and the roller bearing, defined by nodes 32, 33, and 44. The small quantity of heat created at the labyrinth seals was assumed to vary linearly with speed from 2.2 to 11 W, each, for inner-ring speeds from 1000 to 5000 rpm. Heat generated by the cylindrical bearing was assumed to vary with speed and load and was computed using a handbook equation (ref. 13).

Four independent lubrication systems were considered in the rig model (fig. 7). The two outermost loops (nodes 46, 42, 43 and 48, 40, 41) represent lubricant delivered to the axial and radial hydrostatic thrust bearings, respectively. The two innermost loops (nodes 45, 38, 39 and 50, 36, 37) simulate the lubricant delivered to the test and support bearings. Flow rates, delivery temperature, and heat-transfer properties were individually specified for each loop.

Comparison of Experimental Measurements with Performance Predicted by Spherbean

The test rig model was used to generate system performance data at the operating conditions listed in table I. Every combination of load and speed documented in reference 12 was not simulated. Steady-state thermomechanical performance was examined, with the operating bearing clearance computed as a function of speed, interference fit, pressure, and operating temperature. Measured dimensions of the four bearings used for tests and simulation are given in table II. The five operating parameters used for comparison of measured and calculated performance are defined in table III.

The computed operating parameters are generated as single-valued functions. Physical reality imposes a diffusion of that uniqueness. This could be simulated, for example, by exploring the effect of dimension tolerance extremes, material property variations, and heat-transfer coefficient differences. Computer predicted bearing performance would then be represented by a "bandwidth," not a line. However, the extent and the crosscoupling of these variations within the load support system precludes full exploration within the scope of this effort. Therefore, a minimum ±5 percent bandwidth should be assumed to surround the computerized results presented.

No repeat-run experimental data were available and, thus, the absolute bandwidth spread, which represents experiment-to-experiment parameter variations, is unknown. Based on the measured results, it is prudent to assume that, for a particular test bearing, the experimental temperature bandwidth will be at least ±5 percent of the minimum temperature value.

Calculated predictions and experimental values obtained under pure radial load of 6672 N (1500 lb) are presented for comparison in figure 8. Computed cage-to-shaft speed ratios were all within 2 percent of the measured values investigated and are, therefore, not graphically displayed. This close correlation occurs because of the limited roller slip.

Figure 8 shows that the computed system temperatures are within 3 percent of measured values for shaft speeds to 5000 rpm. The largest difference between measured and calculated temperatures (3.5° C) is found at the inner ring (fig. 8(a)), at 1000 rpm. Lubricant outlet temperature predictions are within 4 percent of measured values for speeds to 5000 rpm.

The comparison of experimental and calculated temperature data in figure 8 was made over an operating speed range having an upper bound near the bearing manufacturer's recommended

TABLE I. - TEST CONDITIONS SIMULATED IN REFERENCE 11 FOR COMPARISON OF CALCULATED AND MEASURED DATA

Test	Description	Identification number of bearing[a]	Speed, rpm	Applied loads, N (lb)	
				Radial	Axial
A	Pure radial load[b]	02	1000 - 5000	6 672 (1500)	0 (0)
				13 345 (3000)	0 (0)
B	Combined load	02	1000 - 5000	6 672 (1500)	3114 (700)
				13 345 (3000)	4448 (1000)
C	Effect of clearance	01	1000 - 5000	6 672 (1500)	0 (0)
				13 345 (3000)	0 (0)
				6 672 (1500)	3114 (700)
				13 345 (3000)	4448 (1000)
D	Effect of Oscu-lation[b]	03	1000 - 5000	6 672 (1500)	0 (0)
				13 345 (3000)	0 (0)
E	High speed	06	5000 - 20 000	311 (70)	4448 (1000)

[a]Table II lists specific test bearing dimensions.

[b]Results are presented in figs. 8 to 11.

TABLE II. - TEST BEARING (MEASURED) DIMENSIONS USED AS INPUT TO SPHERBEAN

	Bearing identification number			
	01	02	03	04
Inner-ring groove radius[a], mm (in.)	39.774 (1.5659)	39.901 (1.5709)	40.749 (1.6043)	41.300 (1.6250)
Outer-ring groove radius[a], mm (in.)	40.371 (1.5894)	40.350 (1.5886)	40.345 (1.5884)	40.381 (1.5898)
Roller diameter[b], mm (in.)	13.00 (0.5117)	13.00 (0.5118)	13.00 (0.5117)	13.01 (0.5122)
Roller crown radius[b], mm (in.)	39.421 (1.5520)	38.915 (1.5321)	38.918 (1.5322)	38.583 (1.5584)
Roller total length[b],mm (in.)	12.05 (0.4745)	11.97 (0.4713)	11.97 (0.4713)	12.02 (0.4732)
Surface roughness,um (μin.):				
Inner raceway[c]	0.071 (2.8)	0.066 (2.6)	0.069 (2.7)	0.13 (5.1)
Outer raceway[d]	0.277 (10.9)	0.269 (10.6)	0.282 (11.1)	0.14 (5.5)
Roller[e]	0.076 (3.0)	0.076 (3.0)	0.066 (2.6)	0.11 (4.3)
Diametral clearance[f], mm (in.)	0.0991 (0.0039)	0.0749 (0.0029)	0.0762 (0.0030)	0.0749 (0.0029)

[a]Average of two rows.
[b]Average value for three rollers.
[c]Average of three equally spaced readings per row.
[d]Average of three equally spaced readings.
[e]Average of three rollers, three readings each.
[f]Average of three readings.

TABLE III. - PREDICTED AND MEASURED OPERATING PARAMETERS

Parameter	Instrumentation	Program analog
Cage speed	Proximity probe and counter	Direct program output
Inner-ring temperature	Average of simultaneous reading of 4 RTD's	Average temperature of nodes 6 and 7
Outer-ring temperature	Average of simultaneous reading of 4 J-type thermocouples	Average temperature of nodes 12 and 13
Oil outlet temperature	J-type thermocouple	Temperature of node 39
Drag torque	Strain gaged beam on inner ring of radial hydrostatic bearing	Torque computed from program predicted steady-state heat generation rate

"limiting speed." Conventional bearing operation above the limiting speed can result in overheating and thermal seizure. To avoid a possible catastrophic test bearing failure at elevated speeds, Spherbean was used to explore high-speed rig performance before execution of the full-scale tests.

The performance of bearing 06 (table I) was examined over a speed range of 5000 to 20 000 rpm. The peak speed is approximately four times greater than the manufacturer's recommended limiting speed. Two load conditions were simulated: pure radial and pure axial. An average hydrostatic bearing inlet oil temperature of 90° C, a value at least 10° C higher than later used in the actual test series, was chosen to simulate a conservative upper temperature limit of bearing performance.

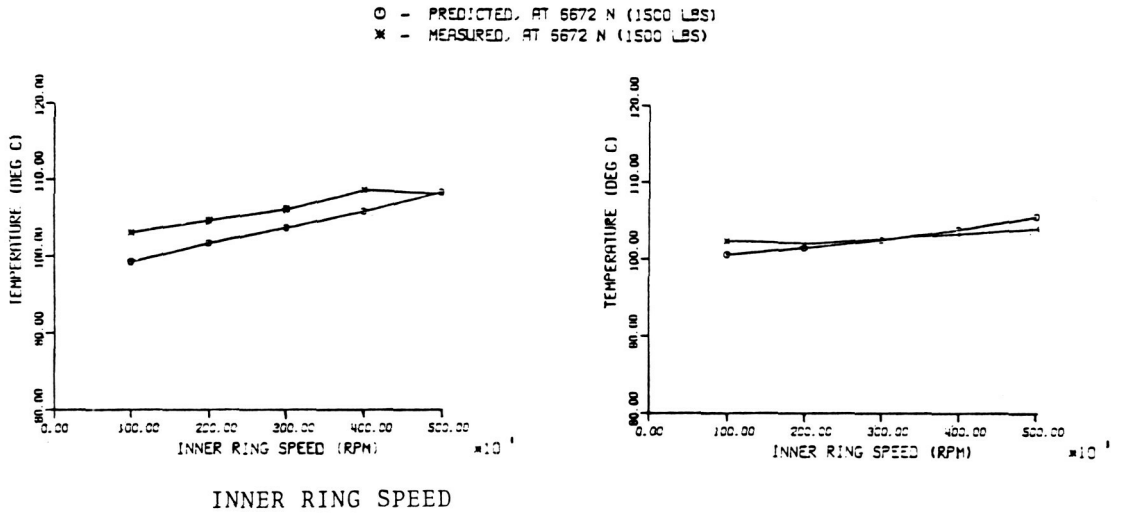

(a) Inner ring temperature comparison.

(b) Outer ring temperature comparison.

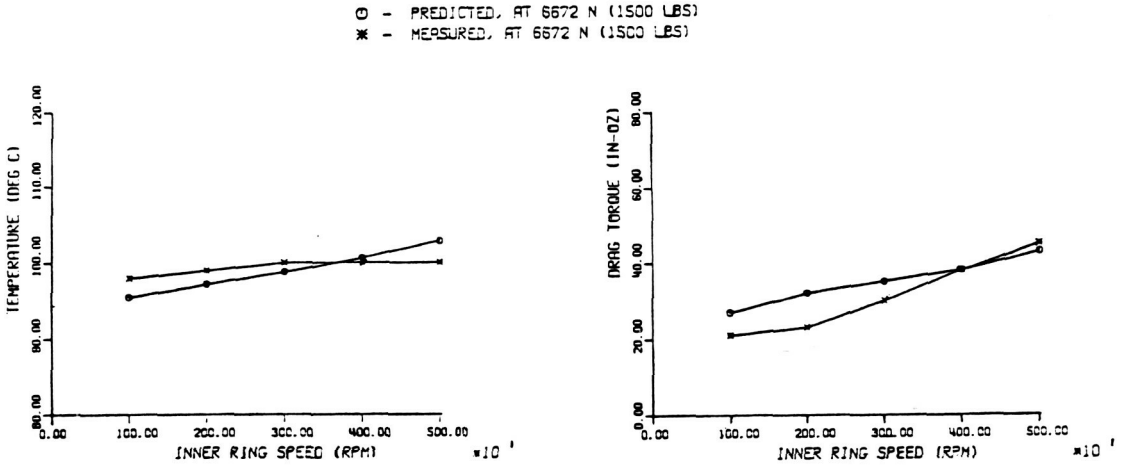

(c) Outlet lubricant comparison.

(d) Drag torque comparison.

Figure 8. - Comparison of predicted and measured data for bearing no. 02 to 5000 rpm. Pure radial load, 6672 N (1500 lb).

Figure 9(a) shows ring temperatures to speeds of 20 000 rpm (0.8 MDN) under a pure axial load of 4448 N (1000 lb). A peak temperature of 195° C is predicted for the inner ring, and 182° C for the outer ring. Both temperatures are well within the material and lubricant oxidation limits.

The bearing diametral clearance remains positive over the speed range investigated (fig. 10(a)). The predicted 0.01-mm loss is attributed to the rise in rolling-element temperature and rotation-induced radial growth of the inner ring. By comparison the 13° C temperature difference between inner and outer rings has a negligible effect (−0.005 mm) on operating clearance.[3]

Film thickness increases 50 percent with speed at the inner ring and 30 percent at the outer ring (fig. 10(a)). The improvement is due to increased rolling velocity, since lubricant viscosity decreases with the higher temperatures encountered at higher shaft speeds.

Predicted ring temperatures under a pure radial load of 13 345 N (3000 lb) are shown in figure 9(b). Peak temperatures of 187° C at the inner ring and 176° C at the outer are achieved at 20 000 rpm. A stable temperature difference of 6° to 11° C is maintained over the entire speed range, and no indications of thermal seizure are seen.

[3]Inner- to outer-ring temperature difference is strongly dependent on the load-support system geometry and lubrication method. It is not likely to be a secondary effect in designs such as pillow blocks or grease lubricated spherical bearings.

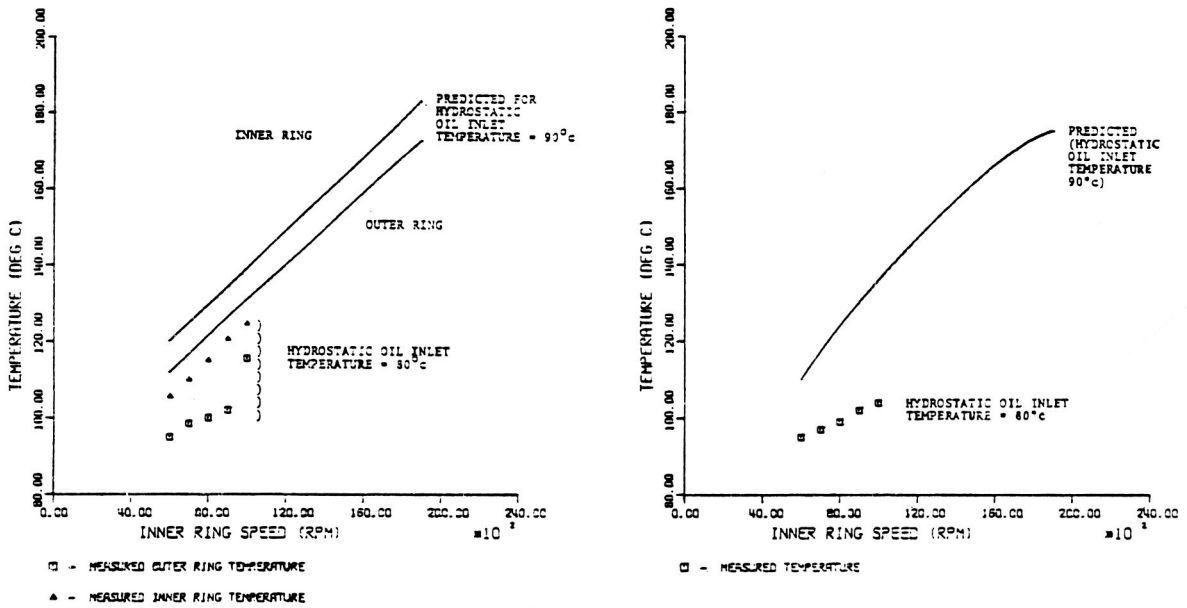

(a) Results under 13 345-N (3000-lb) radial load.

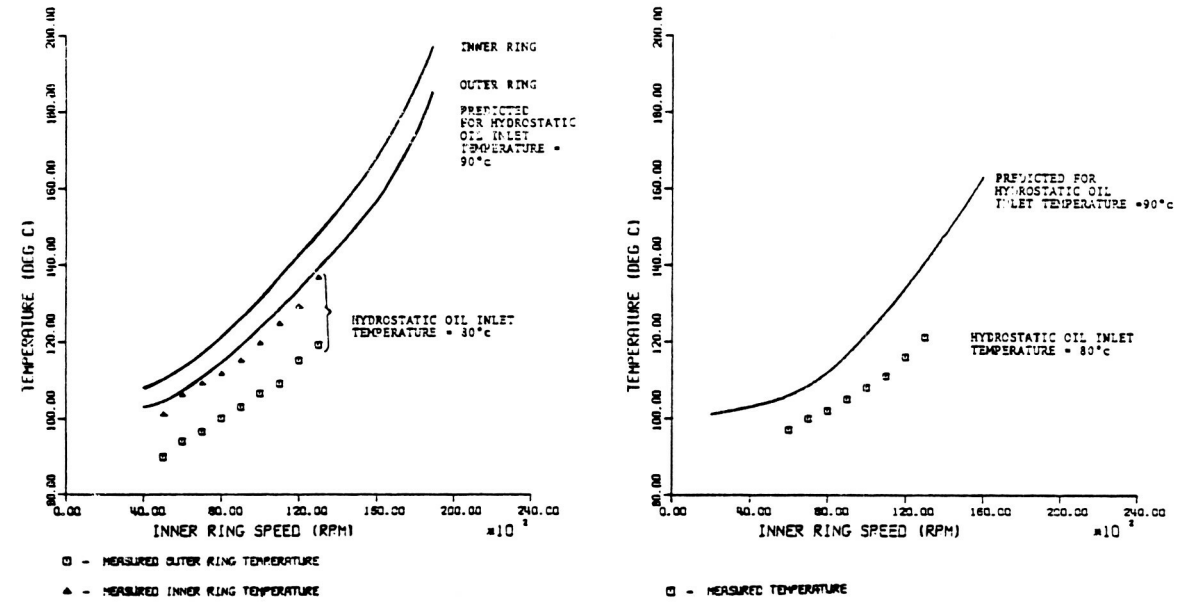

(b) Results under 4448-N (1000-lb) axial load.

Figure 9. - Component temperatures as function of speed to 20 000 rpm (0.8 MDN) under pure axial and pure radial loads.

Bearing diametral clearance remains positive (fig. 10(b)), changing by 18 percent from its initial operating value of 0.056 mm at 6000 rpm. The clearance trend with speed is similar to the trend seen under pure axial load. Clearance change is primarily due to rotation-induced ring growth and heating of the rolling elements.

Film thickness to surface roughness ratio at each raceway increases by 20 percent with speeds to 10 000 rpm, then maintains a nearly constant value to 20 000 rpm (fig. 10(b)).

None of the predicted temperature data to 20 000 rpm were found to indicate a thermal or thermodimensional problem, which may limit the test bearing speed. Also, the predicted cage speed was found to be near epicyclic, indicating that skid would not be a problem.

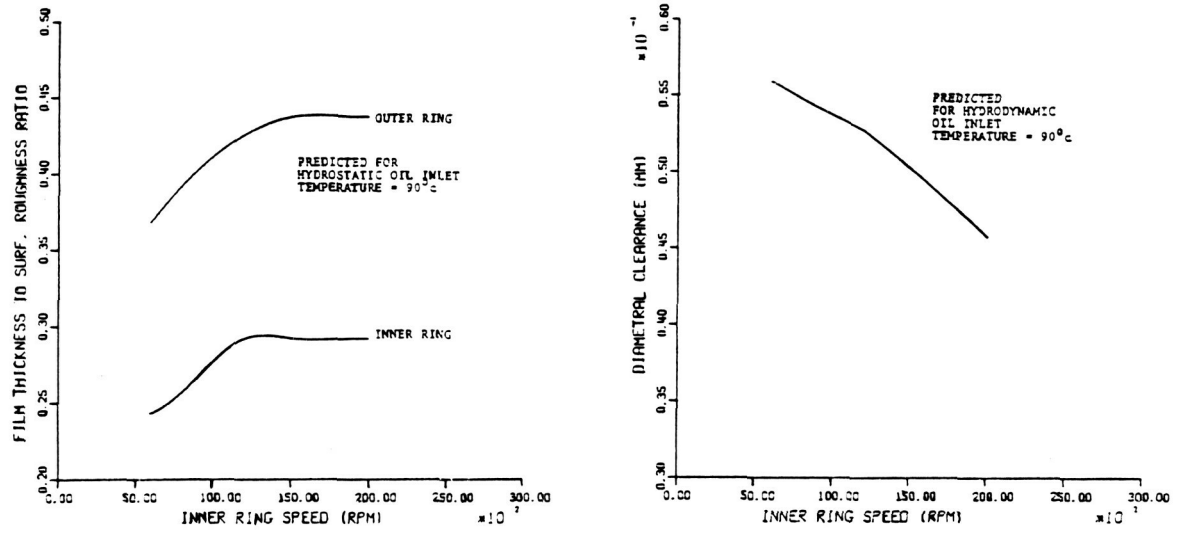

(a) Results under 13 345-N (3000-lb) radial load.

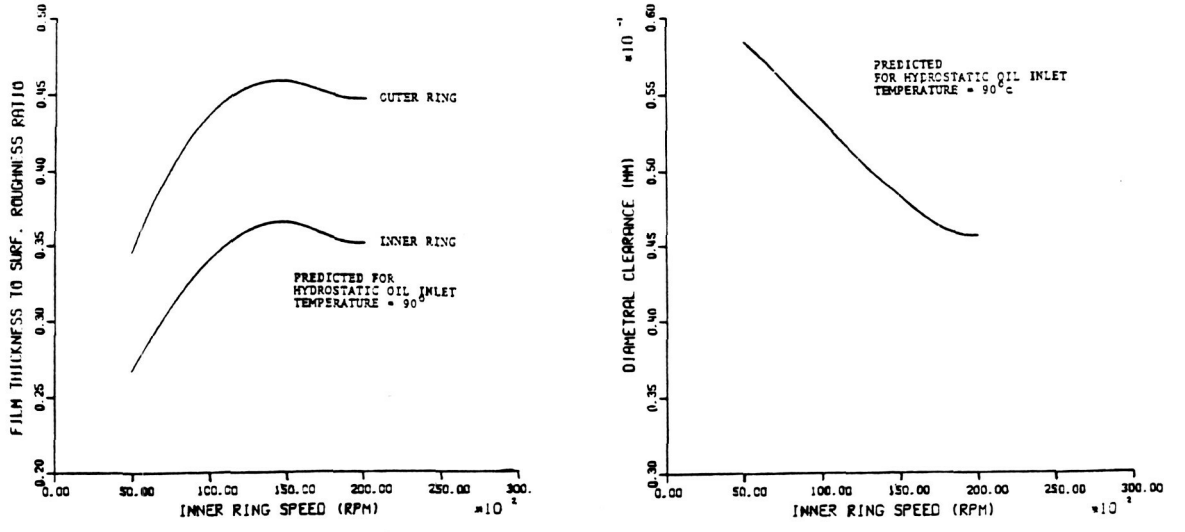

(b) Results under 4448-N (1000-lb) axial load.

Figure 10. - Effect of speed on film thickness and diametral clearance.

During the rig checkout, which followed later, output from the test bearing torque transducer would quit at elevated speeds under each load condition. Therefore, torque data are not available for comparison. The cause for instrument failure was found to be thermal seizure of the radial hydrostatic bearing. Figure 11 shows the program-predicted difference in the radial hydrostatic bearing inner- and outer-ring temperatures (nodes 15 and 17 in fig. 6). The hydrostatic bearing geometry can tolerate an approximately 50° C temperature difference between inner and outer rings before losing all clearance. Referring to figure 11, clearance will be lost, and, therefore, torque transducer output, within the anticipated test speed range.

Design Problem

The example which follows was chosen to demonstrate Spherbean's capability to model roller skew[4] and its effect on bearing performance. Skew was first explored by Kellstrom (ref. 3), who addressed its mechanics and showed how it can effectively provide roller guidance.

[4]Skew refers to rotation of the roller about an axis extending radially outward from the bearing center.

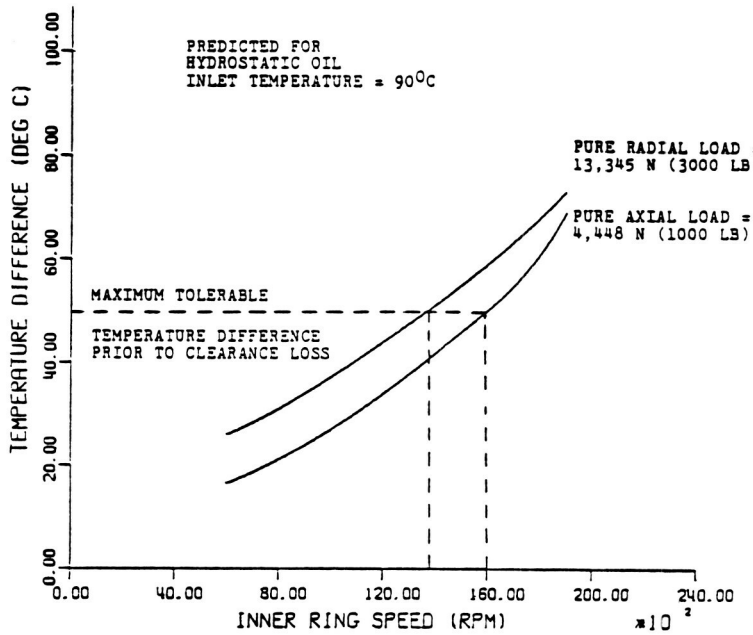

Figure 11. - Calculated temperature difference between inner and outer rings of radial hydrostatic bearings as function of speed.

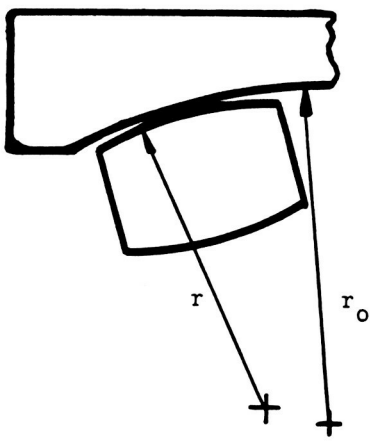

LOOSE CONFORMITY; OSCULATION ∿ .93

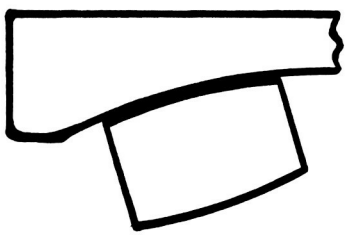

OSCULATION = $\frac{r}{r_o}$

TIGHT CONFORMITY; OSCULATION ∿ .98

Figure 12. - Examples of loose and tight osculations (osculation = r/r_o).

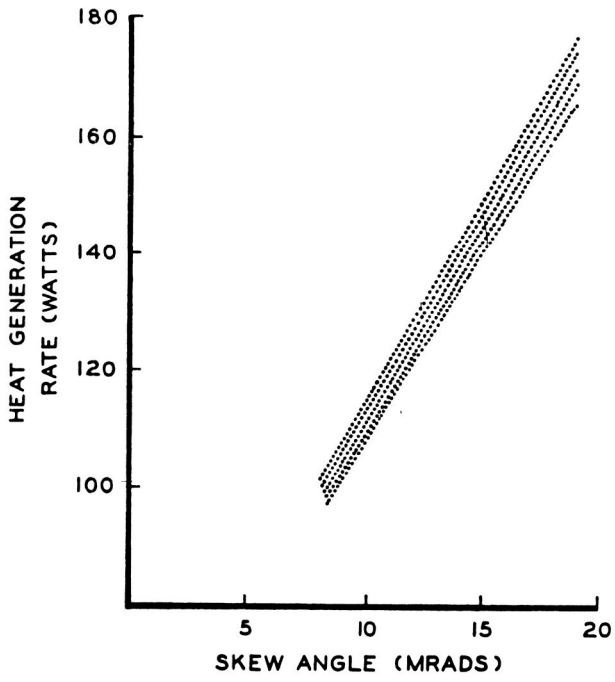

Figure 13. - Relationship between skew angle and power loss.

Skew is affected by several design parameters, including roller and raceway geometry. This is perhaps the simplest practical way to manipulate skew because roller and raceway geometries already receive particular attention during the design process. Currently, a designer may select the geometry only on the basis of contact stress. Geometry resulting in a "loose" conformity (fig. 12) results in a stress peak at the roller center; that resulting "tight" conformity distributes stress, but at the risk of high edge stresses. The designer selects a geometry, lying somewhere between these two extremes, that produces an optimum contact stress field. Thus, a design is achieved by assuming that contact performance is only a function of stress.

Spherbean gives the option of tapping into existing design reserves by exploring performance as a function of several variables. For example, roller-to-raceway sliding at points within the concentrated contact is responsible for 70 percent of the total heat generated by the bearing in the previous example. Power loss heats the bearing components, reduces lubricant effectiveness, and causes a loss of clearance. At very low speed power loss can have minimal effect on performance, but its effect is accentuated with increased speed, and ultimately limits the capability of the bearing.

The effect of roller skew on heat-generation rate was explored at 3000 rpm (0.12 MDN) by simulating bearing performance over a range of outer- and inner-raceway osculations[5] from 0.94 to 0.97. Heat generation was found to increase 60 percent as skew angle increased from 7 to 19 mrad. (fig. 13). The lowest heat-generation rate was found for a combination of high osculation at the outer raceway (0.96) with low osculation at the inner raceway (0.94). The highest heat-generation rate was predicted for low outer- high inner-raceway osculations.

The practical significance of these results, assuming a design goal of a high-speed spherical roller bearing, can be seen in figure 13. A design reserve is tapped by lowering the heat-generation rate from 160 to 100 W. The computer designed bearing can operate at a 33 percent higher speed before generating the same 160 W as a bearing having off-optimum design.

[5]Osculation is the ratio of roller crown radius to raceway groove radius (fig. 12). Typical values lie between 0.93 and 0.98.

References

1. Harris, T. A.: The Effect of Misalignment on the Fatigue Life of Cylindrical Roller Bearings Having Crowned Roller Members, ASME J. Lubr. Techn., vol. 91, no. 2, April 1969, pp. 294-300.
2. Pirvics, J.: The Analysis of Thermal Effects in Rolling Element Bearing Load Support Systems. Proc. 6th Leeds/Lyon Symposium on Tribology at Lyon, Sept. 1979.
3. Kellstrom, E. M.: Rolling Contact Guidance of Roller in Spherical Roller Bearings. ASME Paper No. 79-LUB-23, 1979.
4. Weiland, W. P.; and Poesl, W.: State of the art in Spherical Roller Bearings. SAE Paper No. 790850, 1979.
5. Harris, T. A.; and Broschard, J. L.: Analysis of an Improved Planetary Gear—Transmission Bearing. ASME J. Bas. Eng., Sept. 1964, pp. 457-462.
6. Liu, J. Y.; and Chiu, Y. P.: Analysis of a Planet Bearing in a Gear Transmission System. ASME Paper No. 75-LUB-23.
7. Palmgren, A.: Ball and Roller Bearing Engineering. 3rd Ed., Burbank, 1959.
8. Harris, T. A.: Roller Bearing Analysis, Wiley Inc., 1966.
9. Kleckner, R. J.; and Pirvics, J.: SKF Computer Program SPHERBEAN—Volume I: Analysis. SKF Report No. AT81-D006 (NASA Contract No. NAS3-20824, NASA CR-165203), Jan. 1981.
10. Kleckner, R. J.; and Dyba, G.: SKF Computer Program SPHERBEAN—Volume II: User's Manual. SKF Report No. AT81-D007 (NASA Contract No. NAS3-20824, NASA CR-165204), Jan. 1981.
11. Kleckner, R. J.; Rosenlieb, J. W.; and Dyba, G.: SKF Computer Program SPHERBEAN—Volume III: Program Correlation with Full Scale Hardware Tests. SKF Report No. AT81-D008 (NASA Contract No. NAS3-20824, NASA CR-165205), Jan. 1981.
12. Rosenlieb, J. W.: Appendix A of reference 11, Full Scale Bearing Tests.
13. SKF Industries, Inc., Engineering Data Book, 1973.